

Article

Electric Double Layer Doping of Charge-Ordered Insulators α -(BEDT-TTF) $_2$ I $_3$ and α -(BETS) $_2$ I $_3$

Yoshitaka Kawasaki^{1,2,*}, Hikaru Masuda¹, Jiang Pu³, Taishi Takenobu³, Hiroshi M. Yamamoto^{2,4} , Reizo Kato^{1,2}  and Naoya Tajima¹

¹ Department of Physics, Toho University, Funabashi 274-8510, Chiba, Japan; 5416067m@st.toho-u.jp (H.M.); reizo@riken.jp (R.K.); naoya.tajima@sci.toho-u.ac.jp (N.T.)

² Condensed Molecular Materials Laboratory, RIKEN, Wako 351-0198, Saitama, Japan; yhiroshi@ims.ac.jp

³ Department of Applied Physics, Nagoya University, Nagoya 464-8603, Aichi, Japan; jiang.pu@nagoya-u.jp (J.P.); takenobu@nagoya-u.jp (T.T.)

⁴ Institute for Molecular Science, National Institutes of Natural Sciences, Okazaki 444-8585, Aichi, Japan

* Correspondence: yoshitaka.kawasugi@sci.toho-u.ac.jp

Abstract: Field-effect transistors based on strongly correlated insulators are an excellent platform for studying the electronic phase transition and simultaneously developing phase transition transistors. Molecular conductors are suitable for phase transition transistors owing to the high tunability of the electronic states. Molecular Mott transistors show field-induced phase transitions including superconducting transitions. However, their application to charge-ordered insulators is limited. In this study, we fabricated electric double layer transistors based on quarter-filled charge-ordered insulators α -(BEDT-TTF) $_2$ I $_3$ and α -(BETS) $_2$ I $_3$. We observed ambipolar field effects in both compounds where both electron and hole doping (up to the order of 10^{13} cm $^{-2}$) reduces the resistance by the band filling shift from the commensurate value. The maximum field-effect mobilities are approximately 10 and 55 cm 2 /Vs, and the gate-induced conductivities are 0.96 and 3.6 e^2/h in α -(BEDT-TTF) $_2$ I $_3$ and α -(BETS) $_2$ I $_3$, respectively. However, gate-induced metallic conduction does not emerge. The gate voltage dependence of the activation energy in α -(BEDT-TTF) $_2$ I $_3$ and the Hall resistance in α -(BETS) $_2$ I $_3$ imply that the electric double layer doping in the present experimental setup induces hopping transport rather than band-like two-dimensional transport.

Keywords: organic conductor; charge-ordered insulator; electric double layer transistor; organic field-effect transistor



Citation: Kawasaki, Y.; Masuda, H.; Pu, J.; Takenobu, T.; Yamamoto, H.M.; Kato, R.; Tajima, N. Electric Double Layer Doping of Charge-Ordered Insulators α -(BEDT-TTF) $_2$ I $_3$ and α -(BETS) $_2$ I $_3$. *Crystals* **2021**, *11*, 791. <https://doi.org/10.3390/cryst11070791>

Academic Editor: Toshio Naito

Received: 17 June 2021

Accepted: 4 July 2021

Published: 7 July 2021

Publisher's Note: MDPI stays neutral with regard to jurisdictional claims in published maps and institutional affiliations.



Copyright: © 2021 by the authors. Licensee MDPI, Basel, Switzerland. This article is an open access article distributed under the terms and conditions of the Creative Commons Attribution (CC BY) license (<https://creativecommons.org/licenses/by/4.0/>).

1. Introduction

Strongly correlated insulators at commensurate band fillings, such as the Mott insulator and the charge-ordered insulator, exhibit metal-insulator transitions by shifting the band filling [1]. Intriguing phenomena, such as high-temperature superconductivity and colossal magnetoresistance, emerge in the vicinity of the transition. Band filling control is generally accomplished by chemical substitution. Although this technique can change the band filling over a wide range, it cannot avoid the disorder caused by the introduction of dopants (impurities) and requires different samples for each band filling. Recently, electrostatic doping, which is based on the principle of field-effect transistors (FETs) and can avoid serious impurity effects that may occur in chemical doping, has found widespread use in the study of physical properties [2]. In particular, electric double layer transistors (EDLTs), which use ionic liquids as the gate electrolyte, have been widely adopted in the past decade because they allow a wider range of band filling control than FETs [3,4].

Molecular conductors are a suitable platform for the electrostatic doping of strongly correlated insulators. They contain various strongly correlated insulators and generally form single crystals with clean surfaces. Their lattice constants are generally larger than those of inorganic compounds, so that low electric fields can change large band fillings.

FETs and EDLTs based on molecular Mott insulators have been developed, and field-induced phase transitions have been investigated [5,6]. Studies of the doping effect on charge-ordered insulators have been limited. Yamamoto et al. [7,8] and Kimata et al. [9,10] fabricated FET devices using the charge-ordered insulator α -(BEDT-TTF)₂I₃ and observed decreases in the two-probe resistance between the source and drain electrodes by several tens of percent. However, the charge-ordered state was robust to field-effect doping, and the activation energy was essentially independent of the gate voltage. In this study, we fabricated EDLTs based on α -(BEDT-TTF)₂I₃ and α -(BETS)₂I₃ to investigate dense doping effects on the charge-ordered insulators compared to those in the FET measurements.

2. Materials and Methods

α -(BEDT-TTF)₂I₃ is a quasi-two-dimensional molecular conductor in which the conducting BEDT-TTF layer and the insulating I₃ layer are stacked alternately. Although α -(BEDT-TTF)₂I₃ is a semimetal according to band calculations, and the resistance decreases by cooling, it shows a metal-insulator transition at 135 K [11]. The insulating state is a charge-ordered state in which horizontal charge stripes are formed along the crystallographic *b* axis. The transition temperature is lowered when pressure is applied, and disappears at 1.5 GPa; at this pressure, the Dirac fermion phase emerges [12]. α -(BETS)₂I₃ is the selenium analog of α -(BEDT-TTF)₂I₃. It also shows metal-insulator transition but at a lower transition temperature (\sim 50 K) [13]. Therefore, it is considered that the electronic state of α -(BETS)₂I₃ is similar to that of moderately pressurized α -(BEDT-TTF)₂I₃. However, recent X-ray diffraction and ¹³C nuclear magnetic resonance experiments revealed that α -(BETS)₂I₃ maintains inversion symmetry below the transition temperature [14]. These results imply a different insulating mechanism from simple charge ordering (the spin-orbit interaction may play an important role). The mechanism is still under debate [14–16].

We fabricated EDLTs based on α -(BEDT-TTF)₂I₃ and α -(BETS)₂I₃ by laminating thin single crystals onto polyethylene terephthalate (PET) substrates where Au electrodes were pre-evaporated (Figure 1). The source, drain, and gate electrodes (18 nm thick Au) were patterned on the substrate using photolithography. We electrochemically synthesized thin (\sim 100 nm) single crystals of α -(BEDT-TTF)₂I₃ (α -(BETS)₂I₃) from a chlorobenzene solution of BEDT-TTF (BETS) and tetrabutylammonium triiodide by applying 5 μ A for 20 h. The thin crystal was transferred into 2-propanol with a pipette and guided onto the substrate. After the substrate was removed from the 2-propanol and dried, the crystal adhered to the substrate. Although the X-ray diffraction measurement was difficult, we were able to see through a polarizer that the crystal is a single crystal in which the two-dimensional conducting plane is parallel to the substrate (due to the polarizing property of I₃[−]). As the gate electrolyte, ionic liquid 1-ethyl-3-methylimidazolium 2-(2-methoxyethoxy)ethyl sulfate was dropped to cover both the sample and the gate electrode. Lastly, the EDLT was covered by a 1.2 μ m thick polyethylene naphthalate (PEN) film to reduce thermal stress at low temperatures by thinning the gate electrolyte. After completion, the EDLT was immediately cooled down in a cryostat, and the gate voltage at 220 K was changed to suppress the chemical reaction between the compounds and the ionic liquids. Charge displacement current measurements were performed by sweeping the gate voltage between \pm 0.5 V and measuring the gate current using a source-measure unit (KEITHLEY 2636B, Keithley Instruments, Cleveland, OH, USA). We derived the accumulated surface charge density from

$$p = \frac{Q}{eA} = \frac{\int I_G dV_G}{r_V e A} \quad (1)$$

where I_G , V_G , r_V , e , and A denote the gate current, gate voltage, sweep rate of the gate voltage, elementary charge, and area of the sample, respectively [17]. As for the temperature dependence of the resistance, we employed the standard four-probe method using a DC source (KEITHLEY 2400, Keithley Instruments, Cleveland, OH, USA) and a nano voltmeter (Agilent 34420A, Agilent Technologies, Santa Clara, CA, USA) under various gate voltages. The gate voltage was applied at 220 K in descending order from +0.4 V to −0.4 V in α -

(BEDT-TTF) $_2$ I $_3$ and from +0.8 V to −0.6 V in α -(BETS) $_2$ I $_3$. Beyond those voltage ranges, the sample resistances tended to increase instead, probably because of degradation by the chemical reactions between the ionic liquid and the molecular conductors. The cooling rate was 0.75 K/min, and the data shown were captured during cooling. For α -(BETS) $_2$ I $_3$, we also measured the Hall effect using a superconducting magnet that generates up to 8 T (TeslatronPT, Oxford Instruments, Abingdon, UK).

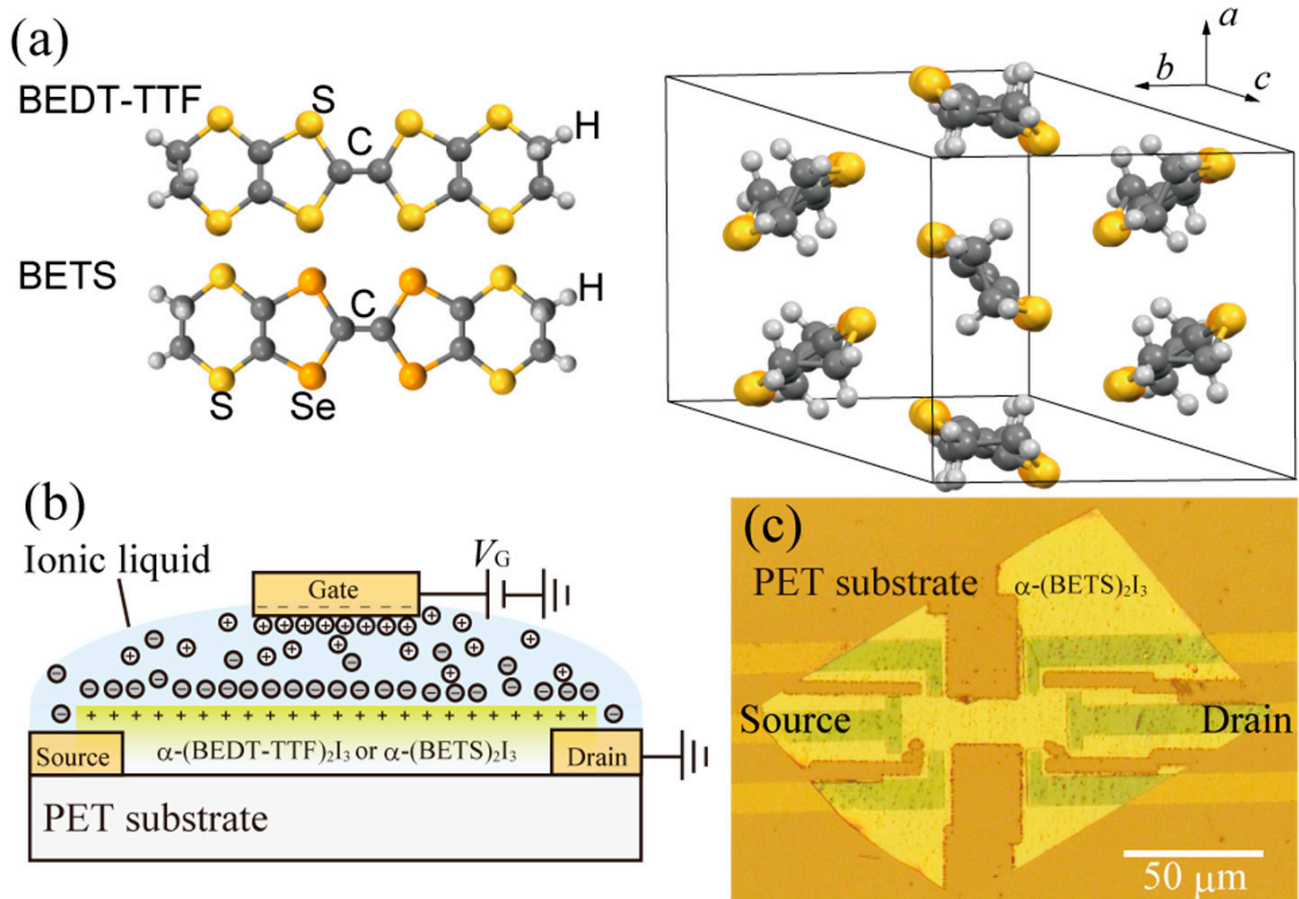


Figure 1. (a) BEDT-TTF and BETS molecules, and crystal structures of α -(BEDT-TTF) $_2$ I $_3$ and α -(BETS) $_2$ I $_3$ (I $_3$ is not shown). (b) Schematic side view and (c) optical top view of an EDLT device. The α -(BETS) $_2$ I $_3$ crystal in (c) is laser-shaped into the Hall bar. The gate electrode (area: 800 \times 800 μ m 2) is patterned on the substrate, a few hundred micrometers away from the crystal in (c).

3. Results

3.1. Charge Displacement Current Measurement

First, we performed charge displacement current measurements at 220 K to confirm the accumulated charge density by electric double layer doping. Figure 2 shows the gate voltage V_G dependence of the charge density p , estimated from Equation (1). To the BEDT-TTF salt, the gate voltage of 0.5 V corresponds to approximately 10% doping (100% doping = 1 electron or hole per 2 BEDT-TTF molecules). Electrons are slightly more likely to be doped than holes at the same magnitude of gate voltage. In the case of the BETS salt, 0.5 V corresponds to only ~3% (hole) and ~5% (electron) doping. For reference, 10% doping corresponds to the gate voltage of approximately 250 V in an FET with a 300 nm thick SiO $_2$ film, which generally exceeds the withstand voltage of the SiO $_2$ film. In our previous study on the electric double layer doping of κ -(BEDT-TTF) $_2$ Cu[N(CN) $_2$]Cl, the doping concentration at 0.5 V reached 20%, and the p - V_G curve was more linear [6].

3.2. Temperature Dependence of Resistance at Various Gate Voltages

3.2.1. α -(BEDT-TTF) $_2$ I $_3$

Figure 3a shows the temperature dependence of the four-probe resistance in the EDLT device based on α -(BEDT-TTF) $_2$ I $_3$ at various gate voltages. The device exhibits metal–insulator transitions at approximately 130 K, which is slightly lower than that for typical bulk α -(BEDT-TTF) $_2$ I $_3$ crystals (135 K). The discrepancy is attributable to the biaxial strain effect that is due to the difference in the coefficient of thermal expansion between α -(BEDT-TTF) $_2$ I $_3$ and the PET substrate. At low temperatures, the substrate shrinks and applies compressive strain to α -(BEDT-TTF) $_2$ I $_3$, resulting in the reduction in the transition temperature [18]. The resistivity above the transition temperature is consistent with typical bulk crystals ($\sim 10^{-2} \Omega \text{ cm}$) if we apply a typical thickness of the crystal (100 nm). Below the transition, the resistivity is lower than that of typical bulk crystals as the transition is moderate, probably because of the suppression of the lattice deformation.

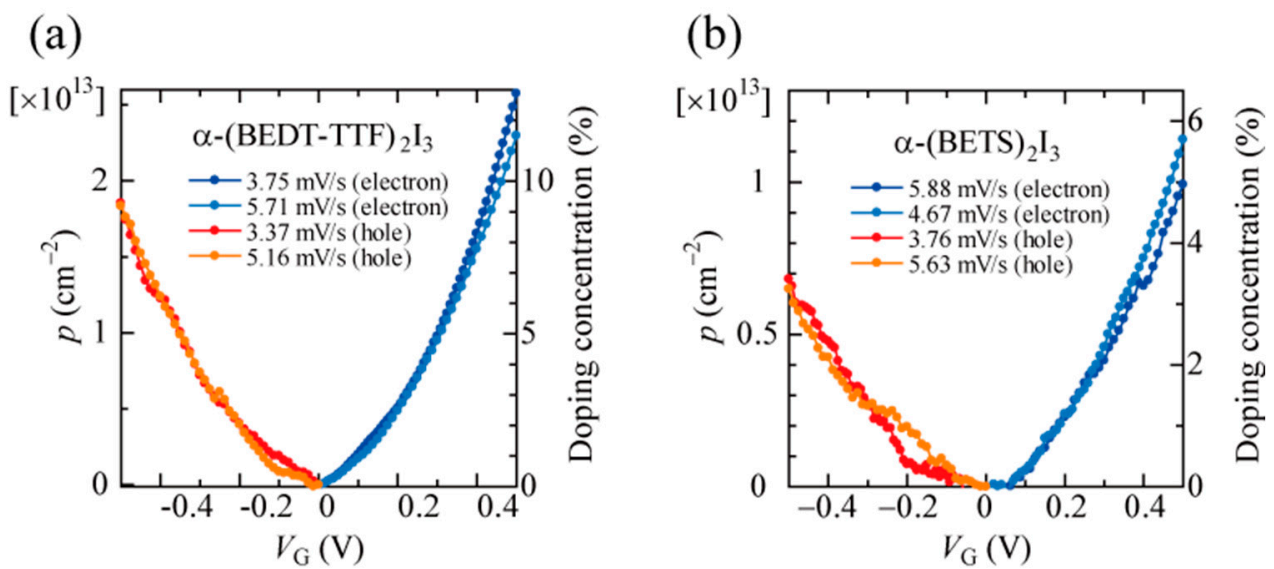


Figure 2. Gate voltage dependence of charge density p in (a) α -(BEDT-TTF) $_2$ I $_3$ and (b) α -(BETS) $_2$ I $_3$ at 220 K.

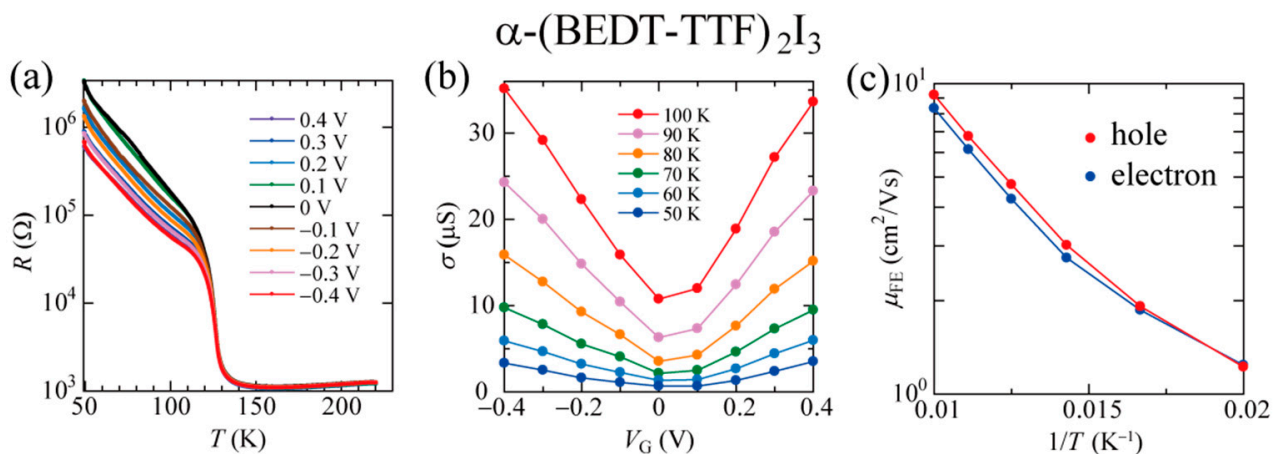


Figure 3. (a) Temperature dependence of the four-probe resistance at various gate voltages in α -(BEDT-TTF) $_2$ I $_3$. (b) Gate voltage dependence of the sheet conductivity at 50–100 K. (c) Arrhenius plots of the field-effect mobility estimated in the range of $0.2 \text{ V} < |V_G| < 0.4 \text{ V}$.

Both positive and negative gate voltages enhance the conductance by up to a few times in the insulating region. The conductance enhancement is more significant than the

case of FET and occurs at the channel (not only at the contacts) because we performed the four-probe measurements. We evaluated the field-effect mobility μ_{FE} , the effective mobility estimated from $\mu_{FE} = (1/C)\partial\sigma/\partial V_G$, where C is the capacitance per unit area of the electric double layer. We roughly estimated C from the slope (linear approximations for $0.2 \text{ V} < |V_G| < 0.4 \text{ V}$) in Figure 2a and obtained $\partial\sigma/\partial V_G$ from the gate voltage dependence of σ (Figure 3b). The derived μ_{FE} is approximately $10 \text{ cm}^2/\text{Vs}$ at 100 K, which is three orders of magnitude higher than those in the FET measurements [9]. μ_{FE} shows similar thermal activation behaviors to the FETs (Figure 3c), although the values are similar for electron and hole in our EDLT. These values are not the actual carrier mobility values. However, they still indicate the switching performance of the resistance.

Nevertheless, as shown in Figures 3a and 4a, the metal–insulator transition temperature remains almost unchanged by the gate voltage, implying that the suppression of the charge ordering by doping, if any, is limited. Generally, the field effect is confined at the sample surface. Our sample consisted of several tens of conducting molecular layers, and the resistance of the bulk was not very high. Therefore, to determine the temperature dependence of the conductance at the doped surface, we had to extract the gate-induced conductance. Figure 4b shows the temperature dependence of the gate-induced sheet conductivity $\Delta\sigma = \frac{L}{W} \left(\frac{1}{R} - \frac{1}{R_{0V}} \right)$ at various gate voltages (where W is sample width, L is sample length). $\Delta\sigma$ monotonically decreased with cooling at all the gate voltages applied in this study, showing no emergence of metallic conduction, and gate-induced melting of charge ordering was unlikely. As shown in Figure 4a,c, neither the non-doped resistance ($V_G = 0 \text{ V}$) nor $\Delta\sigma$ shows simple activation behaviors. Additionally, the variable range hopping mechanism does not describe $\Delta\sigma$ well either. According to Ivek and Čulo [19], the measured resistivity of α -(BEDT-TTF)₂I₃ can be decomposed as $1/\rho_{\text{measured}} = 1/\rho_{\text{NNH}} \mp 1/\rho_{\text{remaining}}$, where ρ_{NNH} is the resistivity of the nearest neighbor hopping (NNH) channel. NNH requires randomly distributed localized states, and ρ_{NNH} depends on the temperature-independent activation energy at low temperatures. However, $\rho_{\text{remaining}}$ depends on the mean-field-like activation energy originating from the charge ordering. In our EDLT device, the Arrhenius plots of $\Delta\sigma$ (Figure 4c) indicate that the activation energy is almost independent of V_G at relatively high temperatures, whereas it is dependent on V_G at low temperatures, as shown in Figure 4d. Assuming that the above two-channel conduction model by Ivek and Čulo [19] applies also to the doped case, we find that the activation energy for the NNH channel, which depends on the average energy difference between the localized states, decreases with gating. In contrast, the activation energy related to charge ordering is not markedly affected by V_G . The doped carriers seemingly fill the disorder-induced localized states and do not significantly prevent the formation of charge ordering.

3.2.2. α -(BETS)₂I₃

Figure 5a,b shows the temperature dependence of the four-probe resistance and the Arrhenius plots for α -(BETS)₂I₃ at various gate voltages. We observed large electron doping effects compared to α -(BEDT-TTF)₂I₃. However, the effects are highly asymmetric against the doping polarity (Figure 5c), where the hole doping slightly reduces the resistance only in the lowest temperature region. μ_{FE} under electron doping is $55 \text{ cm}^2/\text{Vs}$ at 40 K and shows a thermal activation behavior that is similar to the α -(BEDT-TTF)₂I₃ device (Figure 5d). Under electron doping, the gate-induced conductivity $\Delta\sigma$ sufficiently exceeds the Mott–Ioffe–Regel conductivity limit in two dimensions (e^2/h , $\sim 38.7 \text{ } \mu\text{S}$), around which the metallic conduction appears in Si-MOSFET [20] and devices based on κ -type BEDT-TTF salts [21,22]. However, $\Delta\sigma$ in α -(BETS)₂I₃ EDLT does not show metallic conduction below the transition temperature of $\sim 50 \text{ K}$, as shown in Figure 6a. The Arrhenius plots of $\Delta\sigma$ (Figure 6b) show that unlike in α -(BEDT-TTF)₂I₃, the activation energy near the transition temperature significantly decreases with increasing positive V_G . The mechanism is unclear because the insulating state of α -(BETS)₂I₃ is not a simple charge-ordered state, and the

insulating mechanism is under debate [14–16]. However, the present results may provide clues to understanding the insulating phase of this compound.

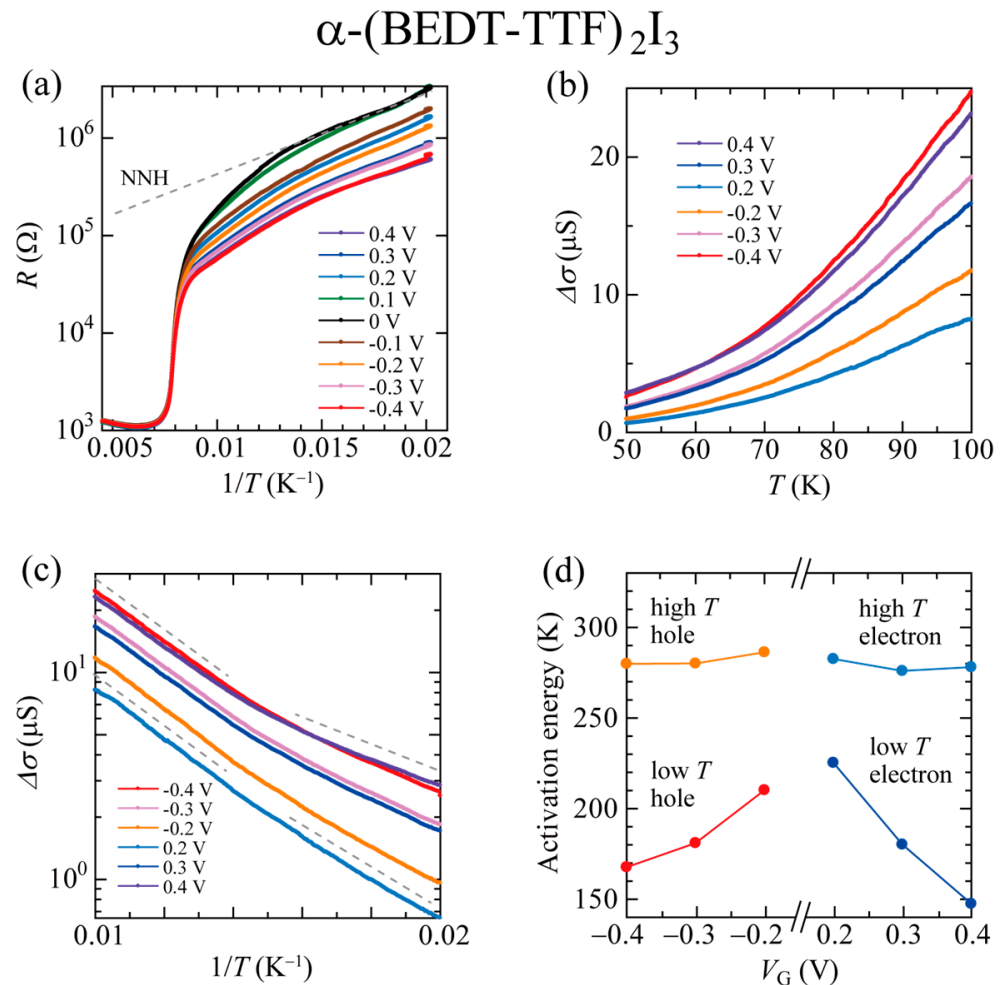


Figure 4. (a) Arrhenius plots of the four-probe resistance at various gate voltages in α -(BEDT-TTF)₂I₃. The dashed line is a guideline of the slope at low temperatures and is assigned to the NNH hopping conduction in the literature. (b) Temperature dependence of the gate-induced sheet conductivity. Note that the data at $|V_G| = 0.1$ V are not shown because $\Delta\sigma = \frac{L}{W} \left(\frac{1}{R} - \frac{1}{R_{0V}} \right)$ contains large errors when R is similar to R_{0V} . (c) Arrhenius plots of the gate-induced conductivity. Dashed lines are guides to the eye. (d) Gate voltage dependence of the activation energy estimated at relatively high (80–100 K) and low (50–60 K) temperatures.

We investigated the Hall effect in α -(BETS)₂I₃ at 10, 5, and 1.7 K, as shown in Figure 7. In order to eliminate any possible influence of magnetoresistance, the Hall resistance R_{xy} was determined as $R_{xy} = [R_{xy}(+B) - R_{xy}(-B)]/2$. Without gating, R_{xy} is positive and proportional to the magnetic field. The slope (= Hall coefficient R_H) increases with cooling, although R_{xy} is unmeasurable at 1.7 K due to the high resistance. R_{xy} decreases by $V_G = 0.2$ V, implying an electron conduction channel on the surface. However, by further electron doping, R_{xy} increases again and almost coincides with the ungated values. We explain below the complicated situation of the Hall effect in our devices [23].

First, R_{xy} of a bulk α -(BETS)₂I₃ crystal is negative. However, thin crystals on PET substrates show positive R_{xy} because hole carriers are doped by contact charging with the substrate. Therefore, two conduction channels (bulk and the α -(BETS)₂I₃/substrate interface) already exist without gating. The gate voltage would induce the third conduction channel (ionic liquid/ α -(BETS)₂I₃ interface). It is difficult to distinguish the contribution of each conduction channel to R_{xy} . Nonetheless, as R_{xy} at $V_G = 0$ V is proportional to the

magnetic field, we can regard the two conduction channels (bulk and bottom interface) as one effective V_G -independent channel. Then, in principle, we can extract the mobility and the carrier density at the gated surface by fitting the data using the formula

$$R_{xy} = \frac{(\mu_0^2 n_0 + \mu_s^2 n_s) + (\mu_0 \mu_s B)^2 (n_0 + n_s)}{e \left[(\mu_0 |n_0| + \mu_s |n_s|)^2 + (\mu_0 \mu_s B)^2 (n_0 + n_s)^2 \right]} B \quad (2)$$

where μ_0 , n_0 , μ_s , and n_s denote the effective mobility and the carrier density at $V_G = 0$ V, and the mobility and the carrier density at the gated surface, respectively. Using the values of μ_0 and n_0 derived from R_{xx} and R_{xy} at $V_G = 0$ V, and the constraint $R_{xx} = 1/e(\mu_0 |n_0| + \mu_s |n_s|)$, we should obtain μ_s and n_s . However, we could not find any realistic solutions that reproduce the nonlinear R_{xy} at 0.2 V. Furthermore, assuming for simplicity that R_{xy} is proportional to B (the terms quadratic to B in Equation (2) can be ignored), we obtain hole carriers with $\mu_s = 8.9$ cm²/Vs and $n_s = 6.4 \times 10^{12}$ /cm². These values are obviously inconsistent with the charge injection by the positive gate voltage (Figure 2), implying a large discrepancy between the drift mobility and the Hall mobility. The discrepancy is probably due to hopping or one-dimensional (filamentary) conduction at the doped surface. A possible scenario is that as the gate voltage increases, the hopping or one-dimensionality is strengthened, resulting in R_{xy} becoming consistent with the ungated value as the Hall mobility at the doped surface approaches zero.

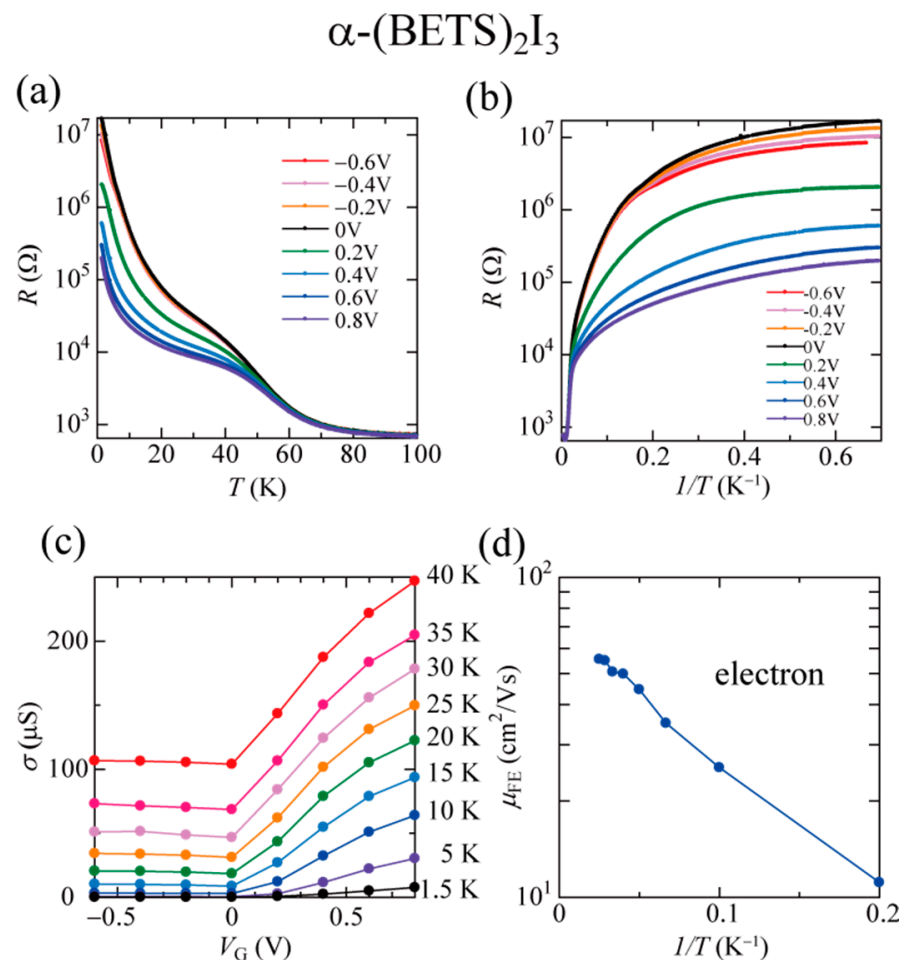


Figure 5. (a) Temperature dependence of the four-probe resistance at various gate voltages and (b) Arrhenius plots for α -(BETS)₂I₃. (c) Gate voltage dependence of the sheet conductivity at 1.5–40 K. (d) Arrhenius plots of the field-effect mobility estimated in the range of 0.2 V < V_G < 0.4 V.

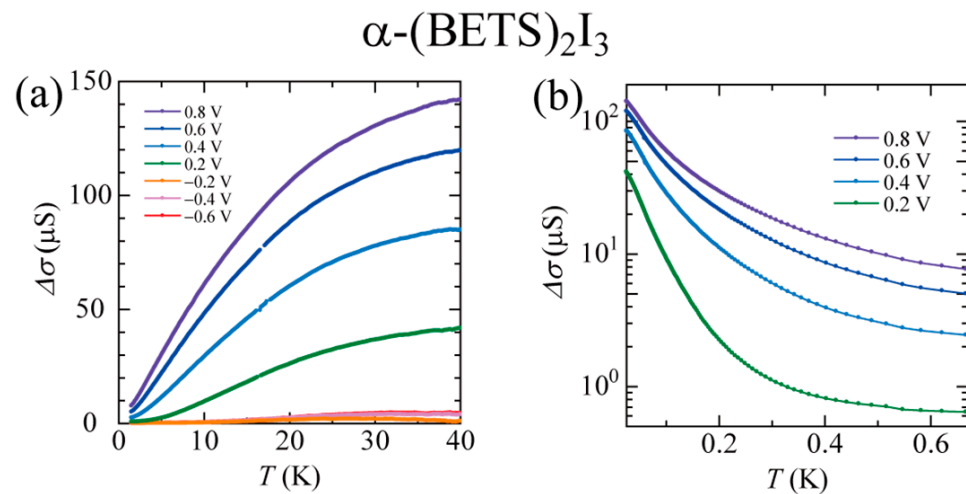


Figure 6. (a) Temperature dependence of the gate-induced conductivity in α -(BETS) $_2$ I $_3$. (b) Arrhenius plots of the gate-induced conductivity.

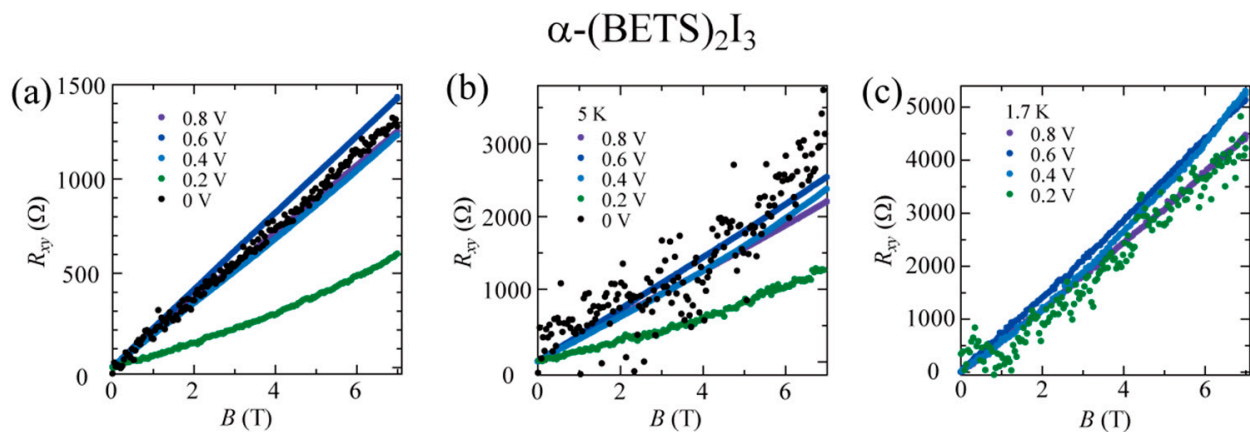


Figure 7. Magnetic field dependence of the Hall resistance under electron doping at (a) 10, (b) 5, and (c) 1.7 K.

4. Discussion and Conclusions

In both compounds, we achieved ambipolar gating effects on the four-probe resistance, indicating that the shift in the band filling in the charge-ordered (and related) insulating state reduces the resistance regardless of the doping polarity. However, we could not observe metallic conduction in the present experimental setup. In α -(BEDT-TTF) $_2$ I $_3$, although the apparent activation energy is significantly decreased by the gate voltage, the extracted gate-induced conductivity implies that only the activation energy for the NNH conduction at low temperatures decreases. The doped carriers fill the randomly distributed localized states (due to the displacement of I $_3^-$ anion chains, according to Ivek and Čulo [19]), and it seems difficult to suppress the charge ordering by further doping in the present device.

In α -(BETS) $_2$ I $_3$, the gate-induced conductivity reaches $\sim 140 \mu\text{S}$, which largely exceeds the Mott–Ioffe–Regel conductivity limit in two dimensions (e^2/h , $\sim 38.7 \mu\text{S}$), around which metallic conduction emerges in various field-effect devices [20–22]. However, we could not observe metallic conduction either. At low electron doping ($V_G = 0.2 \text{ V}$), the Hall resistance significantly decreases (by approximately 50% at 10 K), indicating that the electron doping induces partly two-dimensional, band-like transport at the doped surface. Nevertheless, with increasing gate voltage, the Hall resistance approaches the undoped values, suggesting that hopping or filamentary conduction that hardly contributes to the Hall effect is strengthened. Recently, we observed the Shubnikov–de Haas oscillations in

thin single crystals of α -(BETS)₂I₃ doped by contact charging [23]. Although the doping concentration is comparable ($\sim 10^{12}$ cm⁻²), we could not observe the oscillations in the present device, indicating that the present device has a more disordered surface.

Our results contrast those in Mott EDLTs based on κ -type BEDT-TTF salts, where gate-induced metal–insulator transitions and the Hall effect correspond to the reconstructed Fermi surface. However, the situation in this study may be somewhat typical for the electrolyte gating of organic molecular materials. In rubrene EDLTs, both the field-effect mobility and the Hall mobility generate peaks against the gate voltage [24]. Gate voltage application induces charge carriers at the surface. However, with increasing V_G , the accumulated ions start to form clusters with potential minima that trap the gate-induced carriers [25]. This phenomenon is considered unavoidable in materials with low dielectric constants and narrow bandwidths. To observe more intrinsic field effects, the combination with pressure may be effective because it generally increases the bandwidth. More essentially, the development of a surface treatment method for molecular conductors is necessary to reduce the unevenness of the potential at the gated surface.

Author Contributions: Conceptualization, Y.K. and H.M.Y.; methodology, J.P. and T.T.; investigation and analysis, Y.K., H.M. and N.T.; writing, Y.K., H.M. and N.T.; funding acquisition, Y.K. and R.K. All authors have read and agreed to the published version of the manuscript.

Funding: This research was funded by MEXT and JSPS KAKENHI, grant numbers JP16H06346, JP19K03730, JP19H00891, JP19K15383, JP19K22127, JP20H05664, JP20H05867, 20H05189, and 20H05862. J.P. also acknowledges support from KONDO-ZAIDAN.

Informed Consent Statement: Not applicable.

Data Availability Statement: All data needed to evaluate the conclusions in the paper are presented in the paper. Additional data related to this paper may be requested from the authors.

Acknowledgments: We would like to acknowledge Teijin DuPont Films Japan Limited for providing the PET films and Professor Yutaka Nishio for valuable discussions and advice.

Conflicts of Interest: The authors declare no conflict of interest.

References

1. Imada, M.; Fujimori, A.; Tokura, Y. Metal-insulator transitions. *Rev. Mod. Phys.* **1998**, *70*, 1039–1263. [[CrossRef](#)]
2. Ahn, C.H.; Bhattacharya, A.; Di Ventra, M.; Eckstein, J.N.; Frisbie, C.D.; Gershenson, M.E.; Goldman, A.M.; Inoue, I.H.; Mannhart, J.; Millis, A.J.; et al. Electrostatic modification of novel materials. *Rev. Mod. Phys.* **2006**, *78*, 1185–1212. [[CrossRef](#)]
3. Fujimoto, T.; Awaga, K. Electric-double-layer field-effect transistors with ionic liquids. *Phys. Chem. Chem. Phys.* **2013**, *15*, 8983–9006. [[CrossRef](#)] [[PubMed](#)]
4. Ueno, K.; Shimotani, H.; Yuan, H.; Ye, J.; Kawasaki, M.; Iwasa, Y. Field-induced superconductivity in electric double layer transistors. *J. Phys. Soc. Jpn.* **2014**, *83*, 032001. [[CrossRef](#)]
5. Yamamoto, H.M.; Nakano, M.; Suda, M.; Iwasa, Y.; Kawasaki, M.; Kato, R. A strained organic field-effect transistor with a gate-tunable superconducting channel. *Nat. Commun.* **2013**, *4*, 2379. [[CrossRef](#)]
6. Kawasugi, Y.; Seki, K.; Tajima, S.; Pu, J.; Takenobu, T.; Yunoki, S.; Yamamoto, H.M.; Kato, R. Two-dimensional ground-state mapping of a Mott-Hubbard system in a flexible field-effect device. *Sci. Adv.* **2019**, *5*, eaav7278. [[CrossRef](#)]
7. Yamamoto, H.M.; Ito, H.; Ikeda, M.; Kato, R.; Shigeto, K.; Tsukagoshi, K. Nano-size molecular conductors directly formed on silicon substrates. In *Multifunctional Conducting Molecular Materials*; Royal Society of Chemistry: London, UK, 2006; pp. 97–100.
8. Yamamoto, H.M.; Hosoda, M.; Kawasugi, Y.; Tsukagoshi, K.; Kato, R. Field effect on organic charge-ordered/Mott insulators. *Physica B* **2009**, *404*, 413–415. [[CrossRef](#)]
9. Kimata, M.; Ishihara, T.; Tajima, H. Electrostatic charge carrier injection into the charge-ordered organic material α -(BEDT-TTF)₂I₃. *J. Phys. Soc. Jpn.* **2012**, *81*, 073704. [[CrossRef](#)]
10. Kimata, M.; Ishihara, T.; Ueda, A.; Mori, H.; Tajima, H. Fabrication of a field effect transistor structure using charge-ordered organic materials α -(BEDT-TTF)₂I₃ and α' -(BEDT-TTF)₂I₃Br₂. *Synth. Met.* **2013**, *173*, 43–45. [[CrossRef](#)]
11. Bender, K.; Hennig, I.; Schweitzer, D.; Dietz, K.; Endres, H.; Keller, H.J. Synthesis, Structure and Physical Properties of a Two-Dimensional Organic Metal, Di[bis(ethylenedithiolo)tetrathiofulvalene] triiodide, (BEDT-TTF)⁺₂I⁻₃. *Mol. Cryst. Liq. Cryst.* **1984**, *108*, 359–371. [[CrossRef](#)]
12. Tajima, N.; Sugawara, S.; Tamura, M.; Nishio, Y.; Kajita, K. Electronic phases in an organic conductor α -(BEDT-TTF)₂I₃: Ultra narrow gap semiconductor, superconductor, metal, and charge-ordered insulator. *J. Phys. Soc. Jpn.* **2006**, *75*, 051010. [[CrossRef](#)]

13. Inokuchi, M.; Tajima, H.; Kobayashi, A.; Ohta, T.; Kuroda, H.; Kato, R.; Naito, T.; Kobayashi, H. Electrical and optical properties of α -(BETS)₂I₃ and α -(BEDT-STF)₂I₃. *Bull. Chem. Soc. Jpn.* **1995**, *68*, 547–553. [[CrossRef](#)]
14. Kitou, S.; Tsumuraya, T.; Sawahata, H.; Ishii, F.; Hiraki, K.; Nakamura, T.; Katayama, N.; Sawa, H. Ambient-pressure Dirac electron system in the quasi-two-dimensional molecular conductor α -(BETS)₂I₃. *Phys. Rev. B* **2021**, *103*, 035135. [[CrossRef](#)]
15. Ohki, D.; Yoshimi, K.; Kobayashi, A. Transport properties of the organic Dirac electron system α -(BEDT-TSeF)₂I₃. *Phys. Rev. B* **2021**, *102*, 235116. [[CrossRef](#)]
16. Tsumuraya, T.; Suzumura, Y. First-principles study of the effective Hamiltonian for Dirac fermions with spin-orbit coupling in two-dimensional molecular conductor α -(BETS)₂I₃. *Eur. Phys. J. B* **2021**, *94*, 17. [[CrossRef](#)]
17. Xie, W.; Frisbie, C.D. Organic electrical double layer transistors based on rubrene single crystals: Examining transport at high surface charge densities above 10^{13} cm⁻². *J. Phys. Chem. Rev.* **2011**, *115*, 14360–14368. [[CrossRef](#)]
18. Kawasugi, Y.; Yamamoto, H.M.; Hosoda, M.; Tajima, N.; Fukunaga, T.; Tsukagoshi, K.; Kato, R. Strain-induced superconductor/insulator transition and field effect in a thin single crystal of molecular conductor. *Appl. Phys. Lett.* **2008**, *92*, 243508. [[CrossRef](#)]
19. Ivek, T.; Čulo, M. Semimetallic and charge-ordered α -(BEDT-TTF)₂I₃: On the role of disorder in dc transport and dielectric properties. *Phys. Rev. B* **2017**, *96*, 075141. [[CrossRef](#)]
20. Kravchenko, S.V.; Kravchenko, G.V.; Furneaux, J.E.; Pudalov, V.M.; D’Iorio, M. Possible metal-insulator transition at $B=0$ in two dimensions. *Phys. Rev. B* **1994**, *50*, 8039–8042. [[CrossRef](#)]
21. Sato, Y.; Kawasugi, Y.; Suda, M.; Yamamoto, H.M.; Kato, R. Critical behavior in doping-driven metal–insulator transition on single-crystalline organic Mott-FET. *Nano Lett.* **2017**, *17*, 708–714. [[CrossRef](#)]
22. Kawasugi, Y.; Seki, K.; Pu, J.; Takenobu, T.; Yunoki, S.; Yamamoto, H.M.; Kato, R. Non-Fermi-liquid behavior and doping asymmetry in an organic Mott insulator interface. *Phys. Rev. B* **2019**, *100*, 115141. [[CrossRef](#)]
23. Kawasugi, Y.; Masuda, H.; Uebe, M.; Yamamoto, H.M.; Kato, R.; Nishio, Y.; Tajima, N. Pressure-induced phase switching of Shubnikov–de Haas oscillations in the molecular Dirac fermion system α -(BETS)₂I₃. *Phys. Rev. B* **2021**, *103*, 205140. [[CrossRef](#)]
24. Xia, Y.; Xie, W.; Ruden, P.P.; Frisbie, C.D. Carrier localization on surfaces of organic semiconductors gated with electrolytes. *Phys. Rev. Lett.* **2010**, *105*, 036802. [[CrossRef](#)] [[PubMed](#)]
25. Xie, W.; Liu, F.; Shi, S.; Ruden, P.P.; Frisbie, C.D. Charge density dependent two-channel conduction in organic electric double layer transistors (EDLTs). *Adv. Mater.* **2014**, *26*, 2527–2532. [[CrossRef](#)] [[PubMed](#)]